Gate-Controlled Quantum Interference Effects in a Clean Single-Wall Carbon Nanotube $p-n$ Junction

Xiaosong Deng,[1] Kui Gong,[2] Yin Wang,[2] Zebin Liu,[3] Kaili Jiang,[3] Ning Kang,[1,4,*] and Zhiyong Zhang[1,†]

[1]*Key Laboratory for the Physics and Chemistry of Nanodevices and Center for Carbon-based Electronics, School of Electronics, Peking University, Beijing 100871, China*

[2]*Hongzhiwei Technology (Shanghai) Co., Ltd. FL6, BLDG C2, No. 1599, Xinjinqiao Road, PuDong, ShangHai, China*

[3]*State Key Laboratory of Low-Dimensional Quantum Physics, Department of Physics and Tsinghua Foxconn Nanotechnology Research Center, Tsinghua University, Beijing 100084, China*

[4]*Hefei National laboratory, Hefei 230088, China*

(Received 8 March 2022; accepted 13 April 2023; published 17 May 2023)

The precise control and deep understanding of quantum interference in carbon nanotube (CNT) devices are particularly crucial not only for exploring quantum coherent phenomena in clean one-dimensional electronic systems, but also for developing carbon-based nanoelectronics or quantum devices. Here, we construct a double split-gate structure to explore the Aharonov-Bohm (AB) interference effect in individual single-wall CNT $p-n$ junction devices. For the first time, we achieve the AB modulation of conductance with coaxial magnetic fields as low as 3 T, where the flux through the tube is much smaller than the flux quantum. We further demonstrate direct electric-field control of the nonmonotonic magnetoconductance through a gate-tunable built-in electric field, which can be quantitatively understood in combination with the AB phase effect and Landau-Zener tunneling in a CNT $p-n$ junction. Moreover, the nonmonotonic magnetoconductance behavior can be strongly enhanced in the presence of Fabry-Pérot resonances. Our Letter paves the way for exploring and manipulating quantum interference effects with combining magnetic and electric field controls.

DOI: 10.1103/PhysRevLett.130.207002

Owing to their specific electronic structures and properties, carbon nanotubes (CNTs) have offered an attractive platform to explore intriguing quantum phenomena in one-dimensional (1D) electronic systems, as well as for the development of quantum computing devices and integrated circuits [1–8]. Depending on the chirality, CNTs can exhibit either metallic or semiconducting behavior characterized by the energy gap E_g between conduction and valence bands. The cylindrical geometry of a CNT provides a unique structure for enabling the tunability of the energy spectrum with a magnetic field $B_{\parallel}$ parallel to the tube axis due to the Aharonov-Bohm (AB) effect [9]. This provides an additional dimensionality to modulate the electronic properties of CNT devices. As illustrated in Fig. 1(a), the AB phase tunes the quantized line-cut of the Dirac cone along the $k_{\perp}$ direction in k space, resulting in the change of E_g, $\Delta E_g = 2\hbar\nu\Phi/R\Phi_0$ [9]. Here, $\hbar$ is the reduced Planck constant, ν is the group velocity, Φ is flux resulting from $B_{\parallel}$, R is the radius of the CNT, and Φ_0 is the quantum flux. Thus, the application of $B_{\parallel}$ would result in a Φ_0-periodic modulation of the energy gap, causing the corresponding response of conductance. However, the observation of this phenomenon requires ultrahigh magnetic fields to reach one flux quantum Φ_0, such as 50 T for a CNT with 10 nm diameter, being challenging to achieve experimentally [10].

AB interference magnetoresistance oscillations in individual CNT were first observed in large diameter multiwalled carbon nanotubes (MWCNTs) [11]. However, it has been a long-standing controversy in the context of the role of the inner CNTs and the interplay between band structure and quantum interference in the diffusive regime [12–14]. In the Coulomb blockade regime, flux modulation of the energy spectrum and orbital magnetic moments of nanotubes have been investigated by using single electron tunneling transistors [15,16]. Furthermore, Cao *et al.* [17] considered the effect of $B_{\parallel}$ on interference pattern for single-walled carbon nanotubes (SWCNTs) in the ballistic regime. Despite these investigations, the direct electrical control of the AB effect and strong magnetoresponse at low field in CNT devices remain challenging to achieve. Experimentally, by means of Schottky barriers (SBs) formed at the interface between electrodes and nanotube, the conductance exhibits a modulation with fields [10,18,19]. This band bending profile at the interface is usually determined by the work functions of the contact metal and band structure of nanotube, indicating nearly a fixed SB once the device is fabricated. Moreover, the width of SB is only roughly modulated by the potential, limiting the research of the device transport and physical mechanism in a controllable manner.

 © 2023 American Physical Society

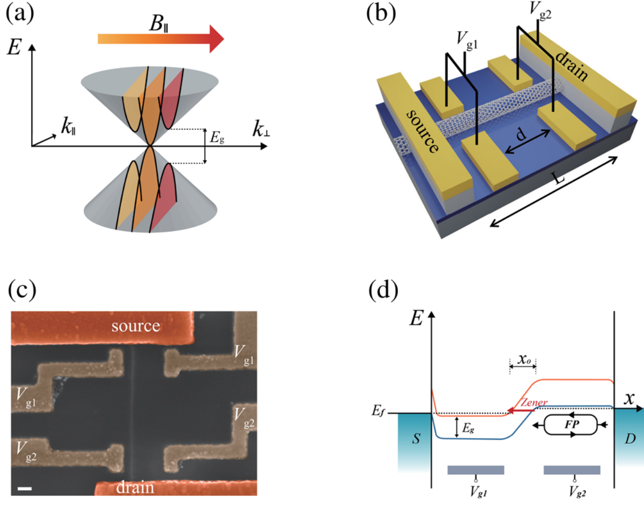

FIG. 1. (a) Energy spectrum of CNT in parallel magnetic field $B_{\|}$ near the Dirac cone. (b) Schematics of the double split-gate device geometry. (c) False-colored SEM image of a representative device. The individual nanotube (gray) is contacted by Pd/Au electrodes (orange) with side gates (brown). Scale bar is 100 nm. (d) Schematic of the potential profile along the channel controlled by V_{g1} and V_{g2}, illustrating the formation of the $p-n$ junction. Landau-Zener tunneling exists in a CNT device under a given bias.

Andreev proposed theoretically a band tunneling model in the CNT $p-n$ junction, in which the conductance modulations can be sensitive to the variation of E_g through the AB effect. Depending on the built-in electric field E_{in} across the junction, the conductance can be tuned by the joint effect of the Landau-Zener tunneling process and AB interference, according to the following relation [20]:

$$G = \frac{2e^2}{h} \exp \sum_{j=1,2} \left[-\frac{\pi \hbar \nu}{4eE_{\text{in}}R^2} \left(\frac{\Delta_0 R}{\hbar \nu} + \frac{(-1)^j \Phi^2}{\Phi_0} \right) \right], \qquad (1)$$

where j is the different valleys, Δ_0 is the energy gap at zero magnetic field (4 from the full energy gap). As a result, a flux modulated magnetoconductance can be achieved at lower field. So far, most AB-modulated transport experiments in SWCNT were still limited in very high magnetic fields, and there is not yet an experimental demonstration of the gate tunable AB effect in a clean CNT device.

In this Letter, we report a low-temperature magnetotransport study in individual CNT $p-n$ junction devices. Being different from the global bottom gate devices in previous works, we design a double split-gate structure to construct an adjustable $p-n$ junction, as depicted schematically in Fig. 1(b). The potential distribution along the channel can be controlled with electrostatic gates, allowing the tunability of electric field across junctions. We observe a modulation of the conductance in parallel magnetic fields, which can be tuned by means of gate voltages. Further angle-dependent measurements provide unambiguous evidence that the observed magnetotransport phenomena is originated from the effect of magnetic flux on the electronic band structure. In addition, we find that the nonmonotonic magnetoconductance response is enhanced due to the presence of Fabry-Pérot resonances.

In this study, CNTs were first grown on Si/SiO_2 substrates by means of chemical vapor deposition (CVD) method [21–23]. The diameters of the CNTs range from 1.5–5.5 nm, determined from atomic force microscope (AFM) height profile (Fig. S1 [24]). Two Pd/Au contact electrodes were defined on the top of the tubes using standard electron-beam lithography and electron-beam evaporation. Finally, four Ti/Au gate electrodes were deposited on the side of the CNT and aligned in pairs to enhance the gate efficiency. Figure 1(c) shows a representative scanning electron micrograph (SEM) of a fabricated device. The distance between the gates and nanotube is varied between 50 and 150 nm. The four CNT devices presented here are all the small gap nanotubes, confirmed by the fitting of the transfer characteristics data using a Landauer model (see Sec. I in the Supplemental Material [24]) [25–28]. During the measurements, the voltages were applied to the split gates to tune the electrostatic potentials on the tube. The structural parameters of the devices can be found in Table I of the Supplemental Material [24]. The electrical transport measurements were performed at a base temperature of 1.9 K equipped with a rotating probe. The magnetic field was applied along the nanotube axis, except for the angle-dependent magnetotransport measurements.

In Fig. 2(a), we display the device conductance as a function of V_{g1} and V_{g2}. It can be seen that this conductance map exhibits a skewed pattern, dividing into four distinct regions. By employing a double split gate structure, we can achieve independent control of carrier density in two adjacent regions. As both V_{g1} and V_{g2} are applied with opposite polarity ($V_{g1} * V_{g2} < 0$), the average conductance of the device is lower than that at the region applied with the same polarity ($V_{g1} * V_{g2} > 0$), indicating the formation of a $p-n$ junction. The conductance fringes in the figure indicate the existence of the interference-enhanced resonances near the junction region as will be discussed later.

Having established the split gates-controlled $p-n$ junction in our CNT device, we now focus on the magnetotransport behavior of the CNT $p-n$ junction. Figure 2(b) shows the evolution of magnetoconductance (MC) for various intensities of the built-in electric field E_{in} near the $p-n$ boundary region. The measurement points of gate voltage are indicated by colored marks on the conductance map in Fig. 2(a). The strength of E_{in} can be tuned by the difference between V_{g1} and V_{g2}, and the rainbow-colored arrow denotes the enhancement of E_{in}. With the increase of the magnetic field from zero, the conductance starts to rise, showing a positive MC, and reaches a maximum at a certain magnetic field. This nonmonotonic behavior is observed for the overall MC

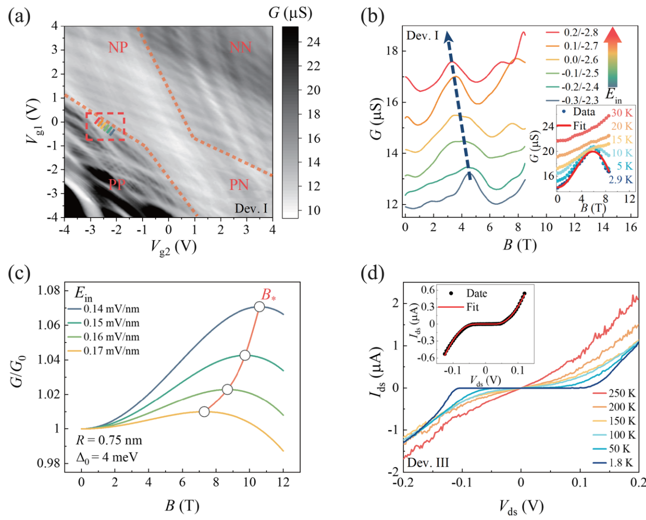

FIG. 2. (a) Conductance G as a function of V_{g1} and V_{g2} at $B = 0$ T and $T = 3.2$ K. Labels denote the charge carrier configuration of the four quadrants defined by split gates. (b) Magnetoconductance traces for different gate voltages, located near the $p-n$ boundary region and indicated by the colored lines in (a). With increasing built-in electric field E_{in}, the magnetoconductance peak moves towards lower magnetic fields. Inset: Temperature evolution of nonmonotonic magnetoconductance. The red line represents the fitting to Eq. (1). (c) E_{in} dependence of calculated magnetoconductance based on the band tunneling model. The hollow circles mark the magnetic field position B_* of conductance maximum. (d) $I-V$ characteristics in a $p-n$ junction region at various temperatures. Inset: a fit of typical $I-V$ curve based on the model of Landau-Zener tunneling.

curves in the vicinity of the $p-n$ configuration region. With increasing E_{in}, the field positions of these MC peaks shift gradually to lower field from 4.5 to 3 T, as indicated by arrows. The same phenomenon can be seen in other devices shown in Fig. S4 [24]. This nonmonotonic MC behavior is highly unusual for 1D conductors. Most previous experiments on CNT devices have observed a monotonic dependence of conductance with field over this low-field range, where the magnetic flux penetrating the nanotube is much smaller than the flux quantum [18,19]. Since the conductance of our individual CNT-based devices is greater than 10 μS, the observed MC behavior cannot also be attributed to a resonance effect caused by the magnetic field-modulated energy level shift in the double quantum dots [8].

The inset of Fig. 2(b) presents the MC at various temperatures. The overall conductance gradually increases with rising temperature, while the peak in MC around 6 T stays nearly unchanged up to ∼10 K. Similar evolution of MC with temperature has been reported before in CNTs, and been related to the effect of spin-orbit interaction (SOI) for small diameter nanotubes [29]. However, such a SOI scenario is inconsistent with our results, which shows a nearly unchanged position of conductance peak at low temperature and then a monotonic positive MC developed at high temperature. Based on the gate-induced $p-n$ junction and related features of magnetotransport behavior, here we propose that the nonmonotonic MC can be understood in terms of an interplay between tunneling through the junction and magnetic flux-induced modulation of the electronic band structure. In the presence of the $p-n$ junction, a tilted potential imposed by split gates is built with the width of $x_0 = E_g/eE_{\text{in}}$. When the barrier thickness of junction is thin enough, the Landau-Zener tunneling process across the junction can be enabled under the biasing condition, and contribute significantly to the device conductance as illustrated in Fig. 1(d).

Andreev has considered the effect of the magnetic field on the Landau-Zener tunneling process in a clean nanotube $p-n$ junction, and predicted a nonmonotonic MC for small gap tubes [20]. Similar nonmonotonic band gap dependence of tunneling current has also been revealed previously in the theoretical study of nanoribbon $p-n$ junctions by considering the band structure and 1D quantum confinement effect in carbon-based nanostructures [30]. In such a scenario, the Landau-Zener tunneling probabilities through junction are strongly dependent on E_g and E_{in}. At given E_{in}, the observed magnetic field dependence of conductance can be understood in terms of the variation of E_g owing to the unidirectional shift of the momentum of electrons by $B_{\parallel}$. Considering the effect of E_{in} on the junction conductance, the potential induced by gating is assumed to be smooth and linear for simplicity [20]. Figure 2(c) demonstrates the calculated conductance at various E_{in} from Eq. (1). Obviously, the enhancement of the E_{in} can drift the characteristic magnetic field B_* for conductance maximum to the lower field, which is consistent with our experimental results shown in Fig. 2(b). The influence of R and Δ_0 is also shown in Fig. S5. Interestingly, even a little change in E_{in} as small as 0.01 mV/nm can result in a significant variation of B_*, significantly enhancing the magnetic response of conductance. The origin of this effect is that the AB phase acts not only on the energy gap by $E_g = \Delta_0 \pm 2\hbar\nu\Phi/R\Phi_0$, but also on the effective length of the Zener tunneling by $x_0 = E_g/eE_{in}$. Therefore, a nonmonotonic magnetoconductance response can be achieved in this Letter at a much lower magnetic field by manipulating AB interference effects with combining magnetic and electric field controls.

Because of the competition between thermal activation and tunneling process, the temperature regime for the appearance of nonmonotonic MC is given in the form, $T < eE_{\text{in}}R$ [20]. Therefore, we can estimate the characteristic temperature scale $T^* \sim 9.5$ K from the fitting to Eq. (1), being consistent with the observed temperature evolution of MC, as shown in the inset of Fig. 2(b). A similar effect of the flux on electronic band structure has been also demonstrated in terms of the field dependent SBs [19].

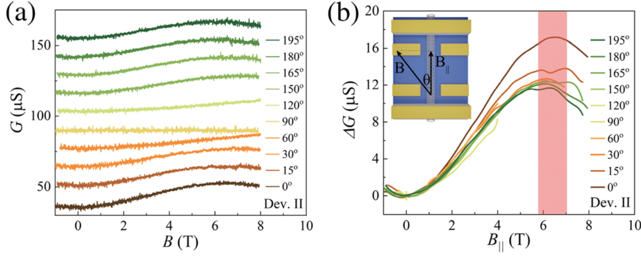

FIG. 3. (a) Magnetoconductance for different titled angles θ. The traces are vertically offset for clarity. (b) The variation of magnetoconductance $\Delta G = G(B) - G(0)$, plotted as a function of axial field, $B_{\parallel} = B\cos\theta$. The peak position of magnetoconductance is found only related to the parallel component of the field. Inset: Schematic of the measurement configuration.

To experimentally fulfill the tunneling potential, they set the measuring point of the devices near the Dirac point, where the injection current dominates the transport. Being distinguished from these studies, the AB-modulated conductance in our devices occur in the doping regions away from the Dirac point. The split-gate geometry allows us to effectively modify the local doping and realize electric control of magnetotransport behavior in CNT devices, compared to other studies using conventional FET structure (summary in Table II and benchmarking in Fig. S6 of Supplemental Material [24]).

Figure 2(d) shows the current-voltage $I-V$ characteristics in a $p-n$ junction region at various temperatures. At high temperatures, the $I-V$ curves are linear with nearly Ohmic characteristics. With decreasing temperatures below 100 K, the $I-V$ behavior becomes apparently non-linear at low bias and develops a weak rectifying behavior, a characteristic of Landau-Zener tunneling. As discussed above, we study the devices with small gap tubes in order to amplify the effect of built-in electric field, which can explain the observed weak rectification characteristic. Thus, the thermal excitation dominates the transport and shunts the tunneling mechanism as $k_B T \sim E_g$, leading to the disappearance of nonlinear $I-V$ and nonmonotonic MC at high temperatures. We model the $p-n$ junction by calculating the tunneling probability based on the Wentzel-Kramer-Brillouin (WKB) approximation [30–32]. The inset of Fig. 2(d) shows a fit of typical $I-V$ curve, which corroborates our experimental data and confirms the occurrence of Zener tunneling in the CNT devices (for details, see Sec. II of the Supplemental Material [24]).

In order to verify the observed nonmonotonic MC originating from the AB phase, we have carried out the angle-dependent measurements. Figure 3(a) displays a series of MC curves for Dev. II at different angles from the same cooldown, taken at $T = 1.9$ K. The angle θ is defined as the tilt angle between the magnetic field and the axial direction of the CNT shown in the inset of Fig. 3(b). As can be seen, when the magnetic field is titled toward the normal direction, the peak of MC gradually moves to

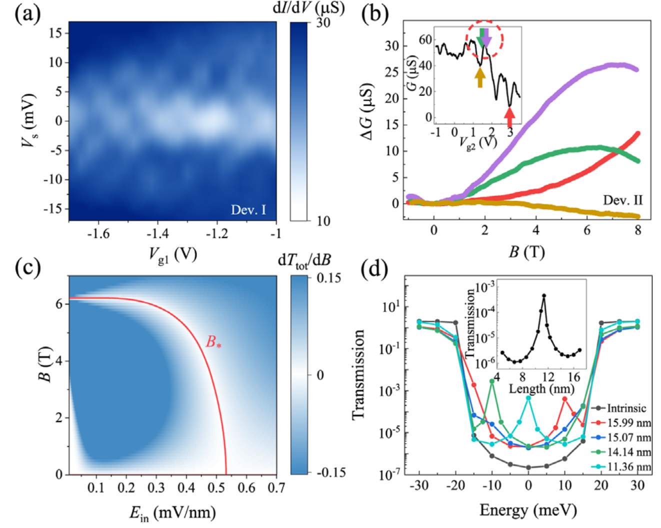

FIG. 4. (a) Color scale plot of dI/dV as a function of V_s and V_{g1}, taken at fixed $V_{g2} = -2.5$ V and $T = 2.9$ K. The spectroscopy exhibits a typical checkerboard pattern for the FP interference. (b) Magnetoconductance traces obtained at different gate voltages corresponding to colored circles in the inset. Inset: Conductance as a function of V_{g2}. The red dotted circles indicate the resonance peaks associated with the appearance of the nonmonotonic magnetoconductance. (c) Calculated differential of total transmission coefficient T_{tot} and magnetic field B as a function of B and E_{in}. The red line is $dT_{\text{tot}}/dB = 0$, namely, B_*. (d) Calculated transmission coefficient of the CNT device, showing an enhancement near the Fermi level in the presence of Zener tunneling. Inset: The transmission coefficient is strongly modulated by varying the length of the doping region.

the higher field. When the magnetic field is applied perpendicular to the CNT ($\theta = 90°$), the MC remains nearly unchanged up to $B = 8$ T, indicating that the vertical field has a negligible effect on magnetotransport. In Fig. 3(b), we plot the variation of conductance ΔG as a function of the parallel component of magnetic field. It can be found that the MC peaks appear at the same magnetic field intensity, while the curve coincides with the others at low fields. Such angle dependence of MC provides unambiguous evidence that only the parallel magnetic field associated with the AB phase contributes to the nonmonotonic magnetotransport behavior, rather than other directionally independent magnetic effects such as *weak localization* or *Zeeman* effect. The same angle dependent MC measurement for Dev. I is shown in Fig. S9.

Finally, we investigate the magnetotransport behavior in the Fabry-Pérot (FP) interference regime. Figure S10 shows the conductance as a function of V_{g2} at varying temperatures and zero magnetic field. As can be seen, the conductance exhibits clearly quasiperiodic oscillations with gating. Considering the high value of conductance ($\sim e^2/h$) for our devices, the observed oscillation features can be understood by phase-coherent transport within the nanotube, leading to resonances in transmission due to quantum

interference. In Fig. 4(a), we display a color scale plot of differential conductance dI/dV as a function of bias voltage V_s and V_{g1}. The transport spectroscopy exhibits a checkerboardlike pattern, which is characteristic of FP interference in 1D ballistic conductors [33,35–37]. From the quantitative analysis of the observed FP resonance (see Sec. III in Supplemental Material [24]), the spatial length of interference $\approx$ 200–400 nm is in good agreement with the geometrical length of gate electrodes. With the double-gate geometry, we can tune the spatial length of FP interference from 100 to 230 nm by varying V_{g2} at fixed V_{g1}.

Figure 4(b) displays the representative MC traces taken at indicated gate voltage points in the inset in which the conductance exhibits FP oscillations. We can find that the feature of MC modulation significantly depends on the resonant states. The nonmonotonic MC is observed only at the gate voltages where the conductance exhibits a resonant peak, whereas the MC evolves monotonically as the gate voltages move to off-resonance positions. The magnitude of ΔG depends also strongly on gate voltage. These results suggest that the nonmonotonic MC could be enhanced in the presence of the resonant transport through junction. So far, most reported studies have demonstrated the AB-related transport phenomena outside the FP region [13–15,18,20]. Our result is also significantly different from the work of Cao *et al.*, in which the MC modulations at the FP resonance are monotonous at low fields, namely, beating effect [17]. We also observed similar FP beating effect in the regime where there is no formation of the $p-n$ junction, while no nonmonotonic MC was observed, as shown in Fig. S13 [24].

In such CNT $p-n$ junction devices, the junction region not only acts as the tunneling barriers, but also introduces a potential step for partially transmitting interface forming FP cavity. For deep analysis, we generalized Andreevs model using multichannel Landauer-Buttiker formalism and S matrices [17,33], where we consider the effect of SOI and FP interference (for details see Sec. IV of the Supplemental Material [24]). We reproduce the experimental data and the simulation result that B_* decreases with the enhancement of E_{in} in Fig. 4(c). Moreover, a damping oscillation characteristics of B_* as a function of V_g with the same period of FP interference can be found shown in Fig. S14 [24]. Therefore, we demonstrate that the presence of FP interference may significantly affect the magnetic response of conductance due to the AB effect, which goes beyond Andreev's model. As gate voltage is located at the resonant position, the electron wave propagates back and forth through the $p-n$ junction interface, where the tunneling probability across the junction is largely increased. As a result, one would expect an enhanced transmission due to constructive interference, amplifying the MC response. The MC response enhanced by the presence of FP interference is also demonstrated in Fig. S16 [24], where B_* decreases as the V_g is close to the resonant peak in one FP period. To demonstrate resonant modulated tunneling, we performed a simulation of individual CNT in the presence of doping region based on non-equilibrium Greens function approach and the density functional theory (NEGF-DFT) [34], as shown in Fig. 4(d). Compared to the intrinsic CNT device, the transmission coefficient near the Fermi level is found to be largely increased by an order of magnitude in the presence of Landau-Zener tunneling through $p-n$ junction. In order to model the resonant modulated transport behavior, the transmission spectrum is calculated with the variable length of n-type doping region and given length of the whole device (for details see Sec. V of the Supplemental Material [24]). As shown in the inset of Fig. 4(d), the transmission coefficient exhibits an oscillating feature with the length of doping region varied by 2 orders of magnitude. These results confirm that FP resonance can enhance the transmission of Landau-Zener tunneling in CNT $p-n$ junction. We also note that a characteristic zero-bias peak (ZBP) structure from the bias dependence of dI/dV was also found at the gates where the nonmonotonic MC occurs shown in Fig. S9 [24]. The formation of ZBP indicates the presence of resonant states, which is further evidence of enhanced transmission coefficients.

In summary, we have demonstrated electrical control of the magnetotransport behavior in clean CNT $p-n$ junction devices. By using a double split-gate geometry, we realized gate-tunable CNT $p-n$ junctions and observed for the first time the Aharonov-Bohm modulation of conductance at low magnetic fields where the flux is much smaller than the flux quantum. The dependence of nonmonotonic magnetoconductance on the built-in electric field and temperature is in qualitative agreement with theoretical prediction. Moreover, we find that the presence of Fabry-Pérot resonances further enhances the magnetic response of conductance. Our Letter not only opens a new way of exploring the quantum interference effect by combining magnetic and electric field controls in 1D electronic systems, but also enables the development of novel electromagnetic CNT devices.

We thank T. Pei for helpful discussions. The device fabrication was performed at Peking Nanofab. We acknowledge support by the National Natural Science Foundation of China (Grants No. 11974026, No. 62225101, and No. U21A6004), and the Innovation Program for Quantum Science and Technology (Grant No. 2021ZD0302600).

[*]Corresponding author.
nkang@pku.edu.cn
[†]Corresponding author.
zyzhang@pku.edu.cn

[1] Ph. Avouris, Z. Chen, and V. Perebeinos, Nat. Nanotechnol. **2**, 605 (2007).

[2] M. M. Shulaker, G. Hills, N. Patil, H. Wei, H. Y. Chen, H. S. Philip Wong, and S. Mitra, Nature (London) **501**, 526 (2013).

[3] E. A. Laird, F. Kuemmeth, G. A. Steele, K. Grove-Rasmussen, J. Nygård, K. Flensberg, and L. P. Kouwenhoven, Rev. Mod. Phys. **87**, 703 (2015).

[4] M. Marganska, L. Milz, W. Izumida, C. Strunk, and M. Grifoni, Phys. Rev. B **97**, 075141 (2018).

[5] O. Lesser, G. Shavit, and Y. Oreg, Phys. Rev. Res. **2**, 023254 (2020).

[6] C. G. Qiu, Z. Y. Zhang, M. M. Xiao, Y. J. Yang, D. L. Zhong, and L. M. Peng, Science **355**, 271 (2017).

[7] L. J. Liu *et al.*, Science **368**, 850 (2020).

[8] J. Waissman, M. Honig, S. Pecker, A. Benyamini, A. Hamo, and S. Ilani, Nat. Nanotechnol. **8**, 569 (2013).

[9] H. Ajiki and T. Ando, J. Phys. Soc. Jpn. **62**, 1255 (1993).

[10] S. H. Jhang, M. Marganska, Y. Skourski, D. Preusche, M. Grifoni, J. Wosnitza, and C. Strunk, Phys. Rev. Lett. **106**, 096802 (2011).

[11] A. Bachtold, C. Strunk, J.-P. Salvetat, J.-M. Bonard, L. Forró, T. Nussbaumer, and C. Schönenberger, Nature (London) **397**, 673 (1999).

[12] A. Fujiwara, K. Tomiyama, H. Suematsu, M. Yumura, and K. Uchida, Phys. Rev. B **60**, 13492 (1999).

[13] S. Roche and R. Saito, Phys. Rev. Lett. **87**, 246803 (2001).

[14] B. Stojetz, C. Miko, L. Forro, and C. Strunk, Phys. Rev. Lett. **94**, 186802 (2005).

[15] U. C. Coskun, T. C. Wei, S. Vishveshwara, P. M. Goldbart, and A. Bezryadin, Science **304**, 1132 (2004).

[16] E. D. Minot, Y. Yaish, V. Sazonova, and P. L. McEuen, Nature (London) **428**, 536 (2004).

[17] J. Cao, Q. Wang, M. Rolandi, and H. J. Dai, Phys. Rev. Lett. **93**, 216803 (2004).

[18] G. Fedorov, B. Lassagne, M. Sagnes, B. Raquet, J. M. Broto, F. Triozon, S. Roche, and E. Flahaut, Phys. Rev. Lett. **94**, 066801 (2005).

[19] B. Lassagne, J. P. Cleuziou, S. Nanot, W. Escoffier, R. Avriller, S. Roche, L. Forro, B. Raquet, and J. M. Broto, Phys. Rev. Lett. **98**, 176802 (2007).

[20] A. V. Andreev, Phys. Rev. Lett. **99**, 247204 (2007).

[21] Z. Jin, H. B. Chu, J. Y. Wang, J. X. Hong, W. C. Tan, and Y. Li, Nano Lett. **7**, 2073 (2007).

[22] X. S. Wang, Q. Q. Li, J. Xie, Z. Jin, J. Y. Wang, Y. Li, K. L. Jiang, and S. S. Fan, Nano Lett. **9**, 3137 (2009).

[23] R. F. Zhang, Y. Y. Zhang, Q. Zhang, H. H. Xie, W. Z. Qian, and F. Wei, ACS Nano **7**, 6156 (2013).

[24] See Supplemental Material at http://link.aps.org/supplemental/10.1103/PhysRevLett.130.207002 for summary of structure parameters for the studied devices, Landauer model fit, additional data of studied devices, Zener model fit, length dependence of the Fabry-Pérot resonances, simulation of the generalized Andreev's model, and simulation of transmission coefficient of the $p-n$ junction, which includes Refs. [17,20,25–34].

[25] Y. Zhao, A. Liao, and E. Pop, IEEE Electron Device Lett. **30**, 1078 (2009).

[26] A. W. Bushmaker, V. V. Deshpande, S. Hsieh, M. W. Bockrath, and S. B. Cronin, Nano Lett. **9**, 2862 (2009).

[27] M. R. Amer, A. Bushmaker, and S. B. Cronin, Nano Lett. **12**, 4843 (2012).

[28] A. Das, S. Pisana, S. Piscanec, B. Chakraborty, S. K. Saha, U. V. Waghmare, R. Yiang, H. R. Krishnamurhthy, A. K. Geim, A. C. Ferrari, and A. K. Sood, Nat. Nanotechnol. **3**, 210 (2008).

[29] S. H. Jhang, M. Marganska, Y. Skourski, D. Preusche, B. Witkamp, M. Grifoni, H. van der Zant, J. Wosnitza, and C. Strunk, Phys. Rev. B **82**, 041404(R) (2010).

[30] D. Jena, T. Fang, Q. Zhang, and H. Xing, Appl. Phys. Lett. **93**, 112106 (2008).

[31] M. R. Amer, S. W. Chang, R. Dhall, J. Qiu, and S. B. Cronin, Nano Lett. **13**, 5129 (2013).

[32] K. Bosnick, A. Gabor, and P. McEuen, Appl. Phys. Lett. **89**, 163121 (2006).

[33] W. J. Liang, M. Bockrath, D. Bozovic, J. H. Hafner, M. Tinkham, and H. Park, Nature (London) **411**, 665 (2001).

[34] J. Taylor, H. Guo, and J. Wang, Phys. Rev. B **63**, 245407 (2001).

[35] A. Javey, J. Guo, Q. Wang, M. Lundstrom, and H. J. Dai, Nature (London) **424**, 654 (2003).

[36] J. Cao, Q. Wang, and H. J. Dai, Nat. Mater. **4**, 745 (2005).

[37] A. V. Kretinin, R. P. Biro, D. Mahalu, and H. Shtrikman, Nano Lett. **10**, 3439 (2010).